

1 **Upper tropospheric water vapour variability at high latitudes**  
2 **– Part 1: Influence of the annular modes**

3 **C. E. Sioris<sup>1\*</sup>, J. Zou<sup>2</sup>, D. A. Plummer<sup>3</sup>, C. D. Boone<sup>4</sup>, C. T. McElroy<sup>1</sup>, P. E. Sheese<sup>2</sup>,**  
4 **O. Moeini<sup>1</sup>, and P. F. Bernath<sup>4,5</sup>**

5 [1] {Department of Earth and Space Science and Engineering, York University, Toronto,  
6 Canada, 4700 Keele St., Toronto, ON, Canada, M3J 1P3}

7 [2] {Department of Physics, University of Toronto, 60 St. George. St., Toronto, ON, Canada,  
8 M5S 1A7}

9 [3] {Canadian Centre for Climate Modelling and Analysis, Environment Canada, Victoria, BC,  
10 Canada}

11 [4] {Department of Chemistry, University of Waterloo, 200 University Ave. W, Waterloo, ON,  
12 Canada, N2L 3G1}

13 [5] {Department of Chemistry & Biochemistry, Old Dominion University, 4541 Hampton Blvd.,  
14 Norfolk, VA, USA, 23529}

15 Correspondence to:

16 C. E. Sioris (csioris@sdcnlab.esse.yorku.ca)

17

18

19

20

21

22

23

24

25

26

27

28

29

30

31

32

33

34

35

36

1 **Abstract**

2 Seasonal and monthly zonal medians of water vapour in the upper troposphere and lower  
3 stratosphere (UTLS) are calculated for both Atmospheric Chemistry Experiment (ACE)  
4 instruments for the northern and southern high-latitude regions (60-90°N and 60-90°S). Chosen  
5 for the purpose of observing high-latitude processes, the ACE orbit provides sampling of both  
6 regions in eight of 12 months of the year, with coverage in all seasons. The ACE water vapour  
7 sensors, namely MAESTRO (Measurements of Aerosol Extinction in the Stratosphere and  
8 Troposphere Retrieved by Occultation) and the Fourier Transform Spectrometer (ACE-FTS) are  
9 currently the only satellite instruments that can probe from the lower stratosphere down to the  
10 mid-troposphere to study the vertical profile of the response of UTLS water vapour to the  
11 annular modes.

12 The Arctic oscillation (AO), also known as the northern annular mode (NAM), explains 64%  
13 ( $r=-0.80$ ) of the monthly variability in water vapour at northern high-latitudes observed by ACE-  
14 MAESTRO between 5 and 7 km using only winter months (January to March, 2004-2013).  
15 Using a seasonal timestep and all seasons, 45% of the variability is explained by the AO at  
16  $6.5\pm 0.5$  km, similar to the 46% value obtained for southern high latitudes at  $7.5\pm 0.5$  km  
17 explained by the Antarctic oscillation or southern annular mode (SAM). A large negative AO  
18 event in March 2013 produced the largest relative water vapour anomaly at 5.5 km (+70%) over  
19 the ACE record. A similarly large event in the 2010 boreal winter, which was the largest  
20 negative AO event in the record (1950-2015), led to >50% increases in water vapour observed by  
21 MAESTRO and ACE-FTS at 7.5 km.

22

23

24

25

26

# 1 1 Introduction

2 Water vapour is the most important greenhouse gas in the atmosphere (Lacis et al., 2010) playing  
3 an important role in climate change by magnifying changes in radiative forcing by longer-lived  
4 greenhouse gases through the water vapour feedback (Dessler and Sherwood, 2009). A variety of  
5 observations have shown that, at near-global scales, specific humidity in the troposphere has  
6 been increasing along with atmospheric temperatures in a manner consistent with that predicted  
7 by the Clausius-Clapeyron equation – approximately 7%/K (Hartmann et al., 2013). Long-term  
8 increases in water vapour are expected in the troposphere due to long-term increases in  
9 temperature and the resulting exponential increase in saturation vapour pressure (Soden and  
10 Held, 2006). In the stratospheric ‘overworld’ (Dessler et al., 1995), long-term changes in water  
11 vapour may result from changes in the temperature of the tropical tropopause ‘coldpoint’ that  
12 controls the dehydration of tropospheric air as it enters the stratosphere (Brewer, 1949) and from  
13 changes in its stratospheric source gas, namely methane (Oman et al., 2008). Water vapour in the  
14 extratropical lowermost stratosphere may be additionally influenced by changes in isentropic  
15 transport from the subtropics (Dessler et al., 2013). Additionally, absorption by atmospheric  
16 water vapour of radiation at terahertz and radio frequencies is a serious impediment for radio  
17 astronomy and for long-distance communications (Suen et al., 2014). The vertical distribution of  
18 water vapour is relevant for all of the effects mentioned.

19 In order to understand and attribute long term changes, internal modes of variability, particularly  
20 those with longer periods, should be considered simultaneously. In the extratropics, the annular  
21 modes explain more of the month-to-month and year-to-year variance of the atmospheric flow  
22 than any other climatic phenomenon (Thompson and Wallace, 2000;  
23 <http://www.atmos.colostate.edu/ao/introduction.html>). The northern and southern annular modes  
24 (NAM, SAM), also known as the Arctic oscillation (AO) and Antarctic oscillation (AAO)  
25 respectively, produce a strong zonal flow at mid-latitudes during their positive phase with an  
26 equatorward meridional flow near 60° latitude, and weaker zonal flow during the negative phase  
27 accompanied by an increased tendency for poleward flow (Fig. 7 of Thompson and Wallace,  
28 2000, Fig. 6 of Boer et al., 2001). Devasthale et al. (2012) used the Atmospheric Infrared  
29 Sounder (AIRS) on the Aqua satellite to study the longitudinal and vertical structure of water  
30 vapour in the 67-82°N band and interpreted the observed structure by separating the observations

1 according to the phases of the Arctic oscillation. The impact of the Arctic and Antarctic  
2 oscillation on upper tropospheric water vapour (UTWV) has been studied by Boer et al. (2001)  
3 using a climate model with atmospheric and oceanic coupling and using the reanalysis data from  
4 the National Centers for Environmental Prediction.

5 The AO exhibits the largest variability during the cold season (Thompson and Wallace, 2000).  
6 Groves and Francis (2002) related TOVS (TIROS Operational Vertical Sounder) precipitable  
7 water vapour net fluxes across 70°N in winter to the phase of the AO. Li et al. (2014) showed  
8 that the longwave radiative forcing anomaly due to NAM-related variability of cold season water  
9 vapour for the 2006 to 2011 period at northern high latitudes is small ( $\sim -0.2 \text{ W/m}^2$ ).

10 Here, the relationship between water vapour in the upper troposphere and lower stratosphere  
11 (UTLS) at northern and southern high-latitudes (60-90°N and 60-90°S) and their respective  
12 annular modes is studied using observations from satellite-based limb profilers. A particular  
13 focus is the height dependence of the relationship: does it extend up to or above the tropopause?

14

## 15 **2 Method**

### 16 **2.1 Satellite observations**

17 SCISAT was launched in 2003 carrying a suite of solar occultation instruments to carry out the  
18 mission named the Atmospheric Chemistry Experiment (ACE) (Bernath et al., 2005). The ACE  
19 instruments measuring water vapour are Measurements of Aerosol Extinction in the Stratosphere  
20 and Troposphere Retrieved by Occultation (MAESTRO, McElroy et al., 2007) and the Fourier  
21 Transform Spectrometer (FTS, Bernath et al., 2005). The ACE datasets begin in February 2004.  
22 The measurements provide a unique combination of high vertical resolution and the ability to  
23 measure the water vapour profile from the mid-troposphere to the lower stratosphere where the  
24 volume mixing ratio (VMR) is  $<10 \text{ ppm}$  (parts per million), below the lower detection limit of  
25 the nadir-sounding AIRS (Gettelman et al., 2004). HIRS (High-Resolution Infrared Radiation  
26 Sounder) is the nadir sounder used in the last two Intergovernmental Panel on Climate Change  
27 (IPCC) assessments (e.g. Hartmann et al., 2013) for long-term trend studies of upper  
28 tropospheric humidity (Soden et al., 2005; Shi and Bates, 2011). However, the trend analysis of  
29 the HIRS dataset is confined to the region 60°N to 60°S (Bates and Jackson, 2001). The

1 Tropospheric Emission Spectrometer (TES) should also be mentioned, but in polar regions at  
2 pressures < 400 mb, the vertical resolution of TES is 11.6 km (Worden et al., 2004). IASI  
3 (Infrared Atmospheric Sounding Interferometer) water vapour retrievals have coarse poor  
4 vertical resolution in the polar upper troposphere and the upper altitude limit of the retrieval only  
5 approaches the tropopause (Herbin et al., 2009; Wiegele et al., 2014). Other current limb  
6 sounders include the sub-millimetre radiometer on Odin which can only measure in the upper  
7 troposphere in the tropics (Rydberg et al., 2009) and the Microwave Limb Sounder on Aura  
8 which can only probe down to 316 mb (~8 km) (Su et al., 2006). The fact that MAESTRO and  
9 ACE-FTS are on the same platform is extremely valuable for comparing the month-to-month  
10 variations of atmospheric constituents observed by both instruments.

11 The MAESTRO water vapour retrieval method follows the one used previously (Sioris et al.,  
12 2010). Data are available at [https://database.scisat.ca/level2/mae\\_water/](https://database.scisat.ca/level2/mae_water/) after user registration.  
13 Some of the main algorithm changes are described here. The maximum allowable optical depth  
14 in the water vapour fitting window (926.0-969.7 nm) is reduced from 7.63 to 6.7. This reduces  
15 the number of noisy spectra but also possibly increases susceptibility to a dry bias at the lowest  
16 altitudes. Also, MODTRAN 5.2 (Berk, 2013 and references therein) is now used for forward  
17 modelling. The water vapour absorption line intensities are mostly from Brown et al. (2002) and  
18 have uncertainties of 2-5%, an improvement relative to the previous version (Sioris et al., 2010)  
19 which used MODTRAN 4 (relying on the HITRAN 1996 spectroscopic database). Water vapour  
20 profiles are retrieved from all available MAESTRO optical depth spectra (version 3.12, spanning  
21 2004 to 2013) from the ongoing ACE mission. For version 3.12 optical depth spectra, the tangent  
22 height registration relies on matching simulated O<sub>2</sub> slant columns obtained from air density  
23 profiles, based on temperature and pressure retrieved from ACE-FTS (Boone et al., 2013), with  
24 slant columns observed by MAESTRO using the O<sub>2</sub> A band. MAESTRO water vapour mixing  
25 ratios that are more than twice as large as all other mixing ratios at any altitude in the same  
26 month were examined in detail and filtered if related to a measurement problem. Significant  
27 outliers are not numerous and no recursion is necessary. No other filtering is necessary. ACE-  
28 FTS gridded version 3.5 data are used in the study. The FTS retrieval is described by Boone et  
29 al. (2013). ACE-FTS water vapour with retrieval uncertainty of >100% are filtered as well as  
30 data points that are significantly negative (i.e. magnitude of mixing ratio is greater than retrieval  
31 uncertainty). Polar Ozone and Aerosol Measurement III (POAM III) water vapour measurements

1 are also used to compare the observed seasonal cycle. Only version 4 data (Lumpe et al., 2006)  
2 with a flag of 0 are used.

## 3 **2.2 Retrieval uncertainties and validation**

4 POAM III has been validated down to 8 km or ~300 mb (Nedoluha et al., 2002; Lumpe et al.,  
5 2006) and this is used as the POAM III lower altitude limit in this work. Previous comparisons  
6 between MAESTRO and ACE-FTS have been favourable (Sioris et al., 2010, Carleer et al.,  
7 2008). ACE-FTS water vapour has been used in the validation of other instruments (e.g. Lambert  
8 et al., 2007) and in the Stratospheric Processes And their Role in Climate (SPARC) Data  
9 Initiative (Hegglin et al., 2013). Waymark et al. (2013) compared version 3 ACE-FTS water  
10 vapour data with the previous well-validated version 2.2 (e.g. Carleer et al., 2008) and found 2%  
11 differences over a large altitude range. Since the MAESTRO tangent height registration has  
12 improved substantially since the previous publication (Sioris et al., 2010), the current version of  
13 MAESTRO water vapour profiles has been validated in a global sense versus ACE-FTS in the  
14 companion paper (Sioris et al., 2015).

15 Beside the validation results, it is also valuable to look at retrieval uncertainties to understand the  
16 expected data quality. Based on an analysis of one year of southern high-latitude data, the  
17 MAESTRO water vapour retrieval relative uncertainty is found to be best at the lowest retrieval  
18 altitude of 5 km and is typically ~30% for a 0.4 km thick layer. The smallest retrieval relative  
19 uncertainty of 2% for ACE-FTS occurs typically at 8.5 km (considering 5.5 to 19.5 km) and  
20 rapidly deteriorates below 7 km to 15% based on northern high-latitude data (2004-2013) on a 1  
21 km altitude grid.

## 22 **2.3 Tropopause definitions**

23 For the northern hemisphere, the monthly tropopause height is defined as the height above 5 km  
24 that is the lower of the lowest local minimum or the lowest height at which the lapse rate is  $<2$   
25 K/km in monthly median temperatures from the Global Environmental Multiscale (GEM)  
26 regional assimilation system (Laroche et al., 1999), sampled on the ACE-FTS 1 km vertical grid.  
27 The lapse rate tropopause concept has been used previously for the extratropics (e.g. Randel et  
28 al., 2012). In the southern hemisphere, due to the winter lower stratosphere being colder than the  
29 tropopause region, the definition is the same except that the lapse rate and lowest local minimum

1 are determined using the monthly maximum temperature profile. Use of monthly median or  
2 mean profiles give tropopauses that reflect the lower stratospheric temperature minimum, where  
3 ozone VMRs are also indicative of lower stratospheric air (i.e. >150 ppm). The same problem is  
4 manifested when using a monthly average of tropopause heights determined from individual  
5 profiles. With the chosen definition, the climatological tropopause at southern high latitudes is at  
6 10.5 km for the winter half of the year (May-October) and at 9.5 km in the summer half  
7 (November to April).

## 8 **2.4 Anomalies**

9 To arrive at water vapour anomalies, there are three steps: creation of the time series (e.g.  
10 monthly or seasonal), compilation of the climatology, and deseasonalization. Monthly time series  
11 are created at northern and southern high latitudes using occultation profiles in the 60-90°N and  
12 60-90°S latitude bands, respectively. The sampling provided by the ACE orbit as a function of  
13 latitude and month is illustrated by Randel et al. (2012). The consequence of the non-uniform  
14 latitudinal sampling as a function of month for the purpose of this study is discussed in Sect. 2.5.  
15 This sampling pattern repeats annually. ACE instruments sample each high latitude region in  
16 only eight of twelve calendar months. November, January, March-May and July-September  
17 represent spring, summer, autumn and winter, respectively, when a seasonal timescale is used in  
18 the southern hemisphere. In the north, climatological values are obtained for all calendar months  
19 except April, June, August, and December. The seasonal anomalies use the following groupings  
20 at northern high latitudes: winter consists of January and February, spring includes March and  
21 May, summer is composed of July and September and the fall is represented by October and  
22 November.

23 Vertically, the binning is done in 1.0 km intervals centered between 5.5 km and 22.5 km (above  
24 23 km, the MAESTRO water vapour absorption signal tends to be below the lower detection  
25 limit). A month is included in the climatology and anomaly dataset at any altitude where  $\geq 20$   
26 observations exist for that given month and altitude. A single MAESTRO profile can supply  
27 more than one observation per altitude bin since the water vapour retrieval is done on the tangent  
28 height (TH) grid, which is as fine as 0.4 km at the lowest TH of 5 km and as the angle widens  
29 between line-of-sight and the orbital track. The same process is followed with ACE-FTS and  
30 POAM III data to generate monthly median and mean time series.

1 The monthly climatology, used to deseasonalize the time series, is generated by averaging the  
2 monthly medians and means over the available years. Figure 1 illustrates the relative difference  
3 between MAESTRO and ACE-FTS water vapour climatologies at both high latitude bands. At  
4 southern high latitudes, monthly means are preferred for Fig. 1 and for the illustrated time series  
5 (Fig. 2) instead of medians which, for MAESTRO, have a dry bias in the widely dehydrated  
6 winter lower stratosphere. However, systematic and seasonally-dependent biases cancel out  
7 given the sensor-specific deseasonalization as discussed at the end of this section, so only  
8 medians are used in the regression analyses (Sect 2.5). An ACE-FTS high bias of  $\sim 10\%$  has been  
9 observed for the extratropical upper troposphere ( $40\text{-}80^\circ\text{N}$  and  $40\text{-}80^\circ\text{S}$ , near 300 hPa) (Hegglin  
10 et al., 2013). While inconclusive, a general wet bias between 5 and 8 km is also suggested by  
11 lidar comparisons in the extratropics (Carleer et al., 2008; Moss et al., 2013). Except below 8 km  
12 where a slight wet bias for ACE-FTS is likely, MAESTRO and ACE-FTS agree within  $\pm 20\%$  at  
13 all heights up to 17.5 km (in 1 km steps) in both hemispheres at high latitudes.

14 The monthly water vapour VMR time series are shown for the southern and northern hemisphere  
15 in Figs. 2 and 3, respectively. At each height, the monthly climatology (e.g., Fig. 4) is subtracted  
16 from the time series (e.g., Fig. 2) to give the absolute deseasonalized anomaly. Dividing the  
17 monthly absolute anomaly by the monthly climatology gives the relative anomaly. Note that July  
18 and August 2011 were omitted from the MAESTRO southern high latitude climatology at 6.5-  
19 9.5 km due to a  $\sim 50\%$  enhancement at these altitudes due to the Puyehue volcanic eruption  
20 (Sioris et al., 2015). The same process is followed to generate anomalies of temperature, relative  
21 humidity (RH), tropopause pressure, and tropopause height. The anomalies of relative humidity  
22 with respect to ice are based on pressure and temperature from the GEM assimilation system and  
23 an accurate saturation vapour pressure formulation (Murray, 1967). The latitude sampling  
24 anomaly is generated by calculating the average sampled latitude for each high-latitude band and  
25 then the mission-averaged latitude in each high-latitude band is subtracted.

26 Note that, because conclusions below about the importance of the annular modes are reached  
27 based on water vapour anomalies and the fact the deseasonalization is sensor-specific (i.e. the  
28 time series observed by each instrument is deseasonalized using its own climatology), constant  
29 biases and seasonally-dependent biases are actually inconsequential. Relevant biases are  
30 discussed in Sect. 2.5.



## 1   **2.5   Regression analysis**

2   We use a multiple linear regression analysis to determine the contribution of the appropriate  
3   annular mode to the variability in deseasonalized water vapour at high latitudes as a function of  
4   altitude. The set of available basis functions include a linear trend, the monthly AAO (Mo,  
5   2000) and AO (Larson et al., 2005) indices (<http://www.cpc.noaa.gov/products/precip/CWlink/>)  
6   and the latitude sampling anomaly time series. This basis function is included to illustrate that  
7   sampling biases are minor even on a monthly time scale (using only the eight months which  
8   sample each high-latitude region). Note that the AO index is calculated following the method of  
9   Thompson and Wallace (2000).

10   When determining the response of water vapour to the AO, the AO index plus a constant are  
11   used, and the linear trend is included if it is significant at the 1 standard error ( $\sigma$ ) level. When  
12   examining trend uncertainty reduction (Sect. 4.2), the regression uses a linear trend, plus a  
13   constant; the annular mode index term is included for trend determination if it improves the trend  
14   uncertainty. Median water vapour anomalies are used in the analysis in both hemispheres since  
15   they respond with smaller uncertainty to the local annular mode than anomalies based on  
16   monthly means.

17   The types of biases that could affect the analysis of water vapour variability are due to:

- 18       1) interannual variation in latitudinal sampling, and
- 19       2) interannual biases in retrieved water vapour profiles.

20   Regarding the non-uniform sampling of latitudes by the ACE orbit mentioned in Sect. 2.4, the  
21   correlation between monthly time series of average sampled latitude in the northern high-latitude  
22   region and the Arctic oscillation index is 0.19 and similarly the correlation between the monthly  
23   time series of average sampled latitude in the southern high-latitude region and the Antarctic  
24   oscillation index is 0.12. Given these very low correlations, ACE's latitudinal sampling should  
25   have a negligible impact on any conclusion about the response of the observed water vapour  
26   anomaly to the annular modes, although this is tested below using the latitude sampling anomaly  
27   as a basis function. Toohey et al. (2013) estimated monthly mean sampling biases in the UTLS to  
28   be  $\leq 10\%$  for the category of instruments that includes ACE-FTS (and MAESTRO). The  
29   interannual biases are also  $< 10\%$  given that Sect. 3.2 below shows that approximately half of the

1 southern high-latitude water vapour seasonal anomaly (typically  $\pm 10\%$  in amplitude) can be  
2 explained by interannual variability in the Antarctic oscillation (i.e. real dynamical variability,  
3 not artificial instrument-related variability). Also, there are no known issues with either  
4 MAESTRO or ACE-FTS specific to a certain year. Furthermore, the self-calibrating nature of  
5 solar occultation, combined with the wavelength stability of spectrometers (relative to filter  
6 photometers) minimize interannual bias for MAESTRO and ACE-FTS. For example, any  
7 variation in the optical (or quantum) efficiency of the instrument does not need to be calibrated  
8 as it does with an instrument measuring nadir radiance.

9

## 10 **3 Results**

11 The MAESTRO water vapour record (Fig. 2) at southern high latitudes is similar to the records  
12 of contemporary limb sounders as shown in Fig. 13 of Hegglin et al. (2013).

### 13 **3.1 Seasonal cycle**

14 The dehydration in September that extends downward into the upper troposphere at southern  
15 high-latitudes (Fig. 4) is clearly observed by MAESTRO annually (Fig. 2).

16 The variability in the UTWV at southern high latitudes on a monthly timescale is dominated by  
17 the seasonal cycle. The observed seasonal variation is a factor of  $\sim 5$  at 8.5 km (Fig. 5). The  
18 seasonal cycle in water vapour is consistent with the ratio of maximum to minimum saturation  
19 vapour mixing ratio at 8.5 km of 4.6 ( $\pm 1$  standard deviation: 3.9-5.3), obtained for a typical year,  
20 namely 2010, using analysis temperatures and pressures from the GEM assimilation system,  
21 sampled at ACE measurement locations for January and August, the months corresponding to the  
22 maximum and minimum water vapour in ACE-FTS and POAM III data at 8.5 km, respectively.

23 The approximate equality between the seasonal cycle amplitudes of observed and saturation  
24 VMR in the troposphere implies a much weaker seasonal cycle in RH. The strong seasonal cycle  
25 in UTWV is in stark contrast to weak (30%) seasonal variations in lower stratospheric (13.5 km)  
26 monthly means, according to MAESTRO observations. The large seasonal cycle amplitude in  
27 saturation vapour mixing ratio in the lower stratosphere is largely due to the extremely cold  
28 temperatures in September.

1 The stronger seasonal cycle at northern high-latitudes (e.g. at 5.5 km, Fig. 6) is partly due to the  
2 non-uniform latitudinal sampling differences in the months of maximum and minimum water  
3 vapour VMR, particularly in the southern hemisphere. The northern hemisphere seasonal cycle  
4 amplitude vertical profile (Fig. 6) is thus a truer reflection of the amplitude of the seasonal cycle  
5 at high latitudes. Figures 5 and 6 illustrate that the seasonal cycle amplitude of observed water  
6 vapour VMR in the lower stratosphere departs from the seasonal cycle amplitude of the  
7 saturation vapour VMR due to the isolation of this overlying atmospheric region from large  
8 sources of water vapour. According to GEM temperature analyses, the amplitude of the seasonal  
9 cycle in temperature is 18 K with a sharp peak in mid-summer (e.g. July) and generally sufficient  
10 to explain the seasonal variation of water vapour VMR and its vertical dependence in the upper  
11 troposphere (Fig. 6).

12 In spite of the large tropospheric seasonality at high latitudes, it is possible to deseasonalize the  
13 water vapour records from the ACE instruments and investigate the remaining sources of  
14 temporal variability, as shown next.

### 15 **3.2 Antarctic oscillation**

16 At 8.5 km, where the largest anti-correlations exist between MAESTRO water vapour at 8.5 km  
17 and the AAO index, it is observed that the relative standard error on the AAO fitting coefficient  
18 is reduced when the regression is performed using a seasonal timescale rather than a monthly  
19 timescale. Thus, in Fig. 7, the MAESTRO and ACE-FTS seasonal median relative anomaly for  
20  $8.5\pm 0.5$  km and  $7.5\pm 0.5$  km, respectively, are presented. The use of medians is preferable for  
21 detecting the annular mode response in the troposphere in both hemispheres since this measure  
22 of central tendency is less susceptible to remaining outliers in the individual retrieved profiles  
23 and because smaller standard errors for the AAO fitting coefficient are obtained. The large  
24 positive anomaly in 2011 is due to the most explosive eruption of a volcano in the last 24 years,  
25 namely Puyehue, and will be discussed in the companion paper (Sioris et al., 2015).

26 At 8.5 km, where the response of water vapour to AAO has the smallest relative  
27 uncertainty for both ACE-FTS and MAESTRO, the response ranges between +23% and -18%  
28 for individual seasons and the standard deviation of the AAO response time series is 10% (2004-  
29 2012). The anomalies in the upper troposphere are highly correlated with each other (e.g.  $R =$

1 0.79 for MAESTRO absolute anomalies at 8.5 versus 9.5 km on a monthly timescale). In the  
2 stratosphere (altitude  $\geq 10$  km), the response of MAESTRO water vapour to AAO is weak (not  
3 significant). Figure 8 illustrates the vertical profile of the AAO response. There is a strong  
4 vertical correlation between the water vapour responses to the AAO observed by the two  
5 instruments and the responses are statistically significant (up to the  $4\sigma$  level for ACE-FTS at 7.5  
6 km) in the 5.5-8.5 km for both instruments indicating that the AAO affects water vapour  
7 throughout the upper troposphere at southern high latitudes. The MAESTRO and ACE-FTS  
8 AAO fitting coefficients are not different from 0 at the  $1\sigma$  level at 10.5 and 11.5 km,  
9 respectively. Slight differences between the ACE instruments may relate to differences in their  
10 respective fields of view (FOV). MAESTRO's FOV is 1 km in the vertical direction, whereas  
11 ACE-FTS, because of its 3.7 km circular field of view at a tangent point 10 km above the  
12 ground, will see some contribution from the troposphere even when the FOV is centered 1.5 km  
13 above the tropopause. Given that the ACE-FTS field of view is circular, the full-width at half-  
14 maximum of the FOV is 3.2 km. Due to vertical oversampling of the FOV, the vertical resolution  
15 of the water vapour products from each ACE instrument is finer than the height of the FOV (see  
16 also Sioris et al, 2010). Nevertheless, differences in vertical resolution between the ACE  
17 instruments will lead to a slight difference in terms of the peak altitude of the anti-correlation  
18 between the water vapour anomaly and AAO. The impact of non-uniform latitudinal sampling is  
19 deferred to Sect. 3.3. The response profile of saturation volume mixing ratio to the AAO is also  
20 shown and is discussed in Sect. 4.3.

### 21 **3.3 Arctic oscillation**

22 Figure 9 shows the altitude dependence of observed water vapour response to the Arctic  
23 oscillation using all eight months that sample the northern high-latitude region. There is a  
24 coherent and statistically significant response (up to the  $4\sigma$  level for MAESTRO) to the AO  
25 observed by both instruments, with a general decrease through the upper troposphere and a  
26 vanishing response in the vicinity of the tropopause. Above 12 km, the response to the AO is  
27 insignificant at the  $1\sigma$  level. The magnitude of the response to the AO is also similar to the  
28 magnitude of the response of UTWV at southern high latitudes to the Antarctic oscillation.

1 The spatiotemporal sampling of ACE (Bernath et al., 2005) is quite non-uniform on monthly  
2 time scales whereas on seasonal timescales the spatial coverage of the entire high-latitude region  
3 becomes more complete. When the latitudinal sampling anomaly is used as a basis function in  
4 fitting monthly water vapour anomaly time series, it is generally not a significant term in either  
5 hemisphere. Fig. 9 shows that the inclusion of this term does not change the response to the AO,  
6 reinforcing the same finding for the response to the AAO (Fig. 8). Clearly, water vapour at high-  
7 latitudes is responding with high fidelity to the local annular mode.

8 Using the MAESTRO water vapour anomalies, a seasonal timestep and all seasons, 45% of the  
9 variability is explained at  $6.5 \pm 0.5$  km, similar to the fraction obtained for southern high latitudes.

10 The most active season for the AO is from January to March based on monthly standard  
11 deviations of the AO index in the period from 1950 to 2015. This three month period was used  
12 by Thompson and Wallace (2000). Figure 10 shows a water vapour anomaly time series for an  
13 altitude of 6.5 km, composed only of January, February and March (2004-2013). The wintertime  
14 anti-correlation between the ACE-FTS water vapour anomaly and the AO index peaks at 6.5 km  
15 with  $R = -0.57$ . MAESTRO shows a much stronger anti-correlation of  $R = -0.80$  at 6.5 and 5.5  
16 km. A large negative AO event in March 2013 produced the largest relative water vapour  
17 anomaly at 5.5 km (+70%) over the MAESTRO record. March 2013 was not available below 8  
18 km for ACE-FTS but at 8.5 and 9.5 km, ACE-FTS and MAESTRO both show the largest  
19 positive anomalies for any March in either northern high-latitude data record (+32 and +35% at  
20 8.5 km and +16 and +27% at 9.5 km for MAESTRO and ACE-FTS, respectively) and a  
21 vanishing enhancement at 10.5 km (above the monthly mean tropopause). A similarly large  
22 event in winter 2010, which was the largest negative AO event in the record (1950-2015), led to  
23 >50% and 30% increases in northern high-latitude water vapour observed at 7.5 km in January  
24 and February 2010, respectively, with agreement between MAESTRO and ACE-FTS. January  
25 2010 has the largest anomaly at 7.5 km in any month (considering all seasons) of the northern  
26 high-latitude data records of MAESTRO and ACE-FTS. Steinbrecht et al. (2011) used a multiple  
27 linear regression analysis to demonstrate a significant increase in total column ozone (+8 Dobson  
28 units) in the winter of 2010 that was attributed to the same historically strong negative phase of  
29 the Arctic oscillation.

30

## 1 **4 Discussion and conclusions**

2 Polar regions have a strong seasonal cycle in UTWV, which is consistent with the seasonality of  
3 the local temperature. The importance of the seasonal cycle in local temperature on UTWV  
4 seasonality at high latitudes has been stated previously (Chen et al., 1999). On the basis of  
5 general circulation model simulations, Del Genio et al. (1994) demonstrated that small-scale  
6 moist convection and the mean meridional circulation have a minor role in the seasonal cycle of  
7 polar UTWV, and that the primary mechanism is eddy moisture fluxes.

8 In the Arctic upper troposphere, condensation and precipitation play a minor role in governing  
9 the water vapour abundance on monthly timescales. Near the Arctic tropopause (250-350 mb),  
10 cloud fractions are <35% (Treffeisen et al., 2007) and MAESTRO monthly median relative  
11 humidity at 9.5 km is < 40% in all 63 months in which this instrument has observed the northern  
12 high-latitude region. However, dynamical variability via the annular modes has been shown here  
13 to strongly affect UTWV at high latitudes. Apart from the seasonal cycle, the Antarctic  
14 oscillation is a dominant mode of variability in upper tropospheric (~8 km) water vapour at  
15 southern high latitudes on a seasonal timescale and the Arctic oscillation explains most of the  
16 variability at wintertime UTWV in northern high latitudes.

### 17 **4.1 Radiative impact**

18 As stated in Sect. 1, the AO is most active in the winter when the surface is coldest. Therefore  
19 less infrared (IR) radiation is emitted and trapped by AO-related increases in atmospheric water  
20 vapour. Over Antarctica, the AAO instead shows strength in late spring (Thompson and Wallace,  
21 2000) at a time when there is increased IR radiation emitted by the surface, possibly making  
22 AAO-related water vapour changes more likely to lead to increases in temperature at the surface  
23 and to reduce outgoing longwave flux at the top of the atmosphere (TOA). The impact of AAO-  
24 induced variability of upper tropospheric water vapour on surface climate and outgoing  
25 longwave flux at the top of the atmosphere is assessed for November 2009 and November 2010,  
26 two months when the AAO was of opposite phase (see Appendix A for details of the method).  
27 The cooling rate differences at the surface between these negative and positive phases of the  
28 AAO are trivial (< 0.07K) in late spring (November). The outgoing longwave flux is reduced by  
29 0.7 W/m<sup>2</sup> in November 2009 relative to November 2010 due solely to AAO-related upper  
30 tropospheric changes in water vapour. Scaling this change to the typical AAO fluctuation in all

1 seasons (1979-2014), variations of  $0.2 \text{ W/m}^2$  are estimated in the outgoing longwave flux at the  
2 TOA, which are equal to the magnitude Li et al. (2014) found for the AO-related IR flux changes  
3 at TOA due to water vapour for the Arctic cold season. Note that Li et al. (2014) found the AO-  
4 related water vapour changes to be much smaller than AO-related cloud changes.

## 5 **4.2 Impact of fitting annular mode indices on decadal trends**

6 In the most recent IPCC report, Hartmann et al. (2013) review the literature on trends in UTWV  
7 observed from satellite instruments. Only one such publication is cited, namely Shi and Bates  
8 (2011). This work uses HIRS data between  $85^\circ\text{N}$  and  $85^\circ\text{S}$ , but only trends at low latitudes  
9 ( $30^\circ\text{N}$ - $30^\circ\text{S}$ ) are discussed. While long-term trends in polar UTWV require continued  
10 measurements and investigation, including the AO index in the trend analysis improves trend  
11 uncertainties below 12 km over the MAESTRO record (e.g. by 16% at 6.5 km) and reduces a  
12 statistically insignificant ( $1\sigma$ ) but consistent, positive bias in the decadal trend (2004-2013) that  
13 is found when the AO is excluded from the regression model. This bias stems from the two large  
14 negative events in the winters of 2010 and 2013 which lie near the end of the data record. The  
15 trend uncertainty reduction is 22% upon inclusion of the Antarctic Oscillation Index into  
16 regression modelling of the linear trend in water vapour at 8.5 km at southern high-latitudes,  
17 again with no significant impact on the linear trend itself.

## 18 **4.3 Proposed mechanisms**

19 The amplitude of the response by water vapour to annular mode oscillations does not change  
20 significantly ( $1\sigma$ ) whether UTWV is binned versus altitude or geopotential altitude in either  
21 hemisphere at high latitudes, indicating the insensitivity to the choice of vertical coordinate. This  
22 is important to note that as the correlation of other atmospheric variables with the annular modes  
23 is explored in this section.

24 There is some observational evidence for two mechanisms that could explain how UTWV at  
25 high latitudes responds to the annular modes. The first is through annular-mode-related air  
26 temperature fluctuations (Thompson and Wallace, 2000), which impact UTWV by changing the  
27 saturation vapour mixing ratio. For changes in saturation vapour mixing ratio to have an impact,  
28 there needs to be an available supply of upper tropospheric water vapour.

1 The second mechanism is through changes to the mean meridional flux itself (e.g. Boer et al.,  
2 2001, Devasthale et al., 2012; Thompson and Wallace, 2000), given the latitudinal gradient in  
3 water vapour between high and mid-latitudes at all upper tropospheric heights. Boer et al. (2001)  
4 have already demonstrated that the response of mean meridional flux of UTWV to the annular  
5 modes using climate model simulations. However, poleward isentropic transport may involve  
6 ascent which may lead to condensation when RH reaches 100%. If sufficient water vapour  
7 condenses, precipitation may occur, which would lower the local VMR of water vapour. But  
8 evaporation and condensation play a minor role in the polar tropospheric water budget (Boer et  
9 al., 2001), with water vapour representing 99% of the total water content (Jakobson and Vihma,  
10 2010, and reference therein). There are many additional, related arguments in favour of the  
11 Eulerian mean meridional circulation as a plausible mechanism to account for the response of  
12 high-latitude UTWV to the annular modes. Firstly, the high-latitude upper troposphere has low  
13 RH (<50%) with the exception of autumn (e.g. March-April in the southern hemisphere).  
14 Secondly, in this autumnal period of higher RH (e.g. 60% below 8 km), the annular mode  
15 activity is low for either hemisphere and conversely, the active period for either annular mode  
16 falls in a season of low RH. Thirdly, the vertical component of the meridional circulation tends  
17 to shift downward during the negative phase of the local annular mode in either hemisphere (Fig.  
18 7 of Thompson and Wallace, 2000), thereby reducing the likelihood of condensation. Fourth, ice  
19 crystals formed during poleward ascending motion will tend to return to the vapour phase before  
20 precipitating, given the dry, surrounding air (e.g. Prospero et al., 1983). Finally, precipitation  
21 may evaporate before descending into the lower troposphere given the vertical gradient in  
22 ambient temperature. These five additional arguments suggest that the meridional flux  
23 mechanism could be effective in transporting water vapour to the high-latitude upper troposphere  
24 on a monthly timescale during the negative phase of the annular mode. Boer et al. (2001) showed  
25 that there is an increased poleward upper tropospheric moisture flux via the meridional mean  
26 circulation at high latitudes during the negative phase of the annular mode in either hemisphere.  
27 According to analysis of Boer et al. (2001), the mean meridional flow mechanism appears to be  
28 of greater relative importance in the high-latitude upper troposphere in the southern hemisphere.  
29 The effectiveness of the mean meridional flux mechanism in increasing UTWV VMR during  
30 negative AAO periods is amplified by the large latitudinal gradients in UTWV between southern  
31 mid and high latitudes. Note that these two mechanisms are not correlated spatially with each



1 other to a high degree. This has been verified using the latitude and altitude dependence of their  
2 responses to the annular modes (Thompson and Wallace, 2000). The two mechanisms are  
3 complementary in that they both increase UTWV at high latitudes during the negative phase of  
4 the local annular mode.

5 There are other mechanisms that are considered such as tropopause variations (discussed below)  
6 and meridional eddy moisture fluxes (Boer et al., 2001). As mentioned above, eddies are  
7 primarily responsible for the seasonal cycle of UTWV (Del Genio et al., 1994). However, Boer  
8 et al. (2001) clearly show for both hemispheres that annular-mode-related moisture fluxes via  
9 eddies are small (relative to the mean meridional flux) and of the wrong sign to explain the  
10 poleward transport of moisture in the high-latitude upper troposphere. However, only the  
11 meridional eddy flux term was considered, whereas Del Genio et al. (1994) point out that large  
12 scale eddies transport moisture upward as well as poleward.

13 We see no evidence in either high-latitude region of a fourth mechanism whereby the UTWV  
14 anomalies are simply explained by annular-mode-driven tropopause variations: the correlation  
15 between tropopause height or tropopause pressure anomalies and the relevant annular mode is  
16 not significant in either high-latitude region ( $-0.1 < R < 0.1$ ). This is not surprising given that the  
17 magnitude of responses of water vapour and saturation vapour VMR to the annular modes  
18 diminish with increasing height toward the tropopause (Figs. 8-9). According to several studies  
19 (e.g. Cai and Ren, 2007; Ambaum and Hoskins, 2002; Highwood et al., 2000), the high-latitude  
20 tropopause tends to rise during the positive phase of the AO. Therefore, the response of the  
21 tropopause to the AO is of the wrong sign to explain increases of UTWV during the negative  
22 phase of the AO.

23 We proceed in this discussion considering only the first two mechanisms since they are  
24 supported by previous studies. The response profile of saturation vapour VMR relative  
25 anomalies (from analyses of the GEM assimilation system) to the AAO (Fig. 8) is studied in  
26 order to isolate and gain insight into the contribution of the first proposed mechanism.

27 Below 9 km, the response of saturation vapour VMR tends to be weaker than the response by  
28 deseasonalized water vapour observed by the ACE instruments, implying that the temperature  
29 mechanism cannot fully explain the strong observed response of water vapour to the AAO at  
30 southern high latitudes (Fig. 8). Near the tropopause (9.5-10.5 km), the response of saturation

1 vapour VMR to the AAO becomes effectively zero (within  $1\sigma$ ), but the response of observed  
2 water vapour to the AAO is also decreasing considerably relative to lower altitudes. The  
3 response of water vapour to the AAO differs significantly between MAESTRO and ACE-FTS  
4 except at 5.5 and 6.5 km, making it generally difficult to unequivocally determine the  
5 contribution of the first proposed mechanism. Nevertheless, there is an obvious need for a  
6 mechanism in addition to the temperature-related one to explain the observed response of water  
7 vapour in the southern high-latitude upper troposphere. This is consistent with the correlation  
8 between the annular mode and mean meridional moisture flux, particularly in the southern  
9 hemisphere (Boer et al., 2001).

10 At northern high latitudes (Fig. 9), saturation vapour VMR responds to the AO in a similar  
11 fashion to its response to the AAO at southern high latitudes. The response of saturation vapour  
12 VMR to the AO at northern high latitudes tends to be smaller in magnitude than the response by  
13 water vapour inferred from ACE observations, but the difference is not statistically significant at  
14 all altitudes compared to the ACE-FTS water vapour response. The water vapour anomalies from  
15 the two ACE instruments show a decreasing response to the AO with increasing altitude at  
16 northern high latitudes, but generally differ in the magnitude of the response, as is the case as  
17 well at southern high latitudes. Thus, no general conclusion can be unequivocally drawn about  
18 the sufficiency of the first proposed mechanism in the northern high-latitude upper troposphere.  
19 The relative contributions by the different mechanisms involved in the response of water vapour  
20 to the annular modes remain uncertain partly due to significant intersensor differences (Figs. 8-  
21 9). Longer datasets and further analysis would be helpful to understand the contribution by the  
22 proposed mechanisms.

23

## 24 **Appendix A: Cooling rate differences**

25 Cooling rate vertical profiles are calculated using MODTRAN5.2 (e.g. Bernstein et al., 1996)  
26 assuming an Antarctic surface altitude of 2.5 km, subarctic summer temperature profile, free  
27 tropospheric aerosol extinction (visibility of 50 km) and two water vapour cases:

28 (1) using MAESTRO climatological median water vapour between 6.5 and 9.5 km increased by  
29 the vertically-resolved water vapour response to AAO determined by multiple linear regression

1 (with AAO and constant as the only predictors) for November 2009, when the AAO was in its  
2 negative phase (index of -1.92).

3 (2) same as (1), except for November 2010, when AAO index was +1.52 (positive phase).

#### 4 **Acknowledgements**

5 The availability of the NOAA annular modes indices is appreciated. The ACE mission is  
6 supported primarily by the Canadian Space Agency. POAM III data were obtained from the  
7 NASA Langley Research Center Atmospheric Science Data Center. CES is grateful to Frédéric  
8 Laliberté (Environment Canada) for a helpful discussion on separating the contributions by the  
9 two mechanisms proposed in Sect. 4.3. The three referees and the editor are thanked for greatly  
10 improving the article.

#### 11 **References**

12 Ambaum, M. H. P., and Hoskins, B. J.: The NAO troposphere–stratosphere connection, *J. Clim.*,  
13 1969-1978, 2002.

14 Bates, J. J. and Jackson, D. L.: Trends in upper-tropospheric humidity, *Geophys. Res. Lett.*, 28,  
15 1695-1698, 2001.

16 Berk, A.: Voigt equivalent widths and spectral-bin single-line transmittances: Exact expansions  
17 and the MODTRAN@5 implementation, *J. Quant. Spectrosc. Radiat. Transfer*, 118, 102-120,  
18 2013.

19 Bernath, P. F., McElroy, C. T., Abrams, M. C., Boone, C. D., Butler, M., Camy-Peyret, C.,  
20 Carleer, M., Clerbaux, C., Coheur, P.-F., Colin, R., DeCola, P., DeMazière, M., Drummond, J.  
21 R., Dufour, D., Evans, W. F. J., Fast, H., Fussen, D., Gilbert, K., Jennings, D. E., Llewellyn, E.  
22 J., Lowe, R. P., Mahieu, E., McConnell, J. C., McHugh, M., McLeod, S. D., Michaud, R.,  
23 Midwinter, C., Nassar, R., Nichitiu, F., Nowlan, C., Rinsland, C. P., Rochon, Y. J., Rowlands,  
24 N., Semeniuk, K., Simon, P., Skelton, R., Sloan, J. J., Soucy, M.-A., Strong, K., Tremblay, P.,  
25 Turnbull, D., Walker, K. A., Walkty, I., Wardle, D. A., Wehrle, V., Zander, R., and Zou, J.:  
26 Atmospheric Chemistry Experiment (ACE): mission overview, *Geophys. Res. Lett.*, 32, L15S01,  
27 doi:10.1029/2005GL022386, 2005.

1 Bernstein, L. S., Berk, A., Acharya, P. K., Robertson, D. C., Anderson, G. P., Chetwynd, J. H.,  
2 and Kimball, L. M.: Very narrow band model calculations of atmospheric fluxes and cooling  
3 rates, *J. Atmos. Sci.*, 53, 2887-2904, 1996.

4 Boer, G. J., Fourest, S., and Yu, B.: The signature of the annular modes in the moisture budget, *J.*  
5 *Clim.*, 14, 3655-3665, 2001.

6 Brown, L. R., Toth, R. A., and Dulick, M.: Empirical line parameters of H<sub>2</sub><sup>16</sup>O near 0.94 μm:  
7 Positions, intensities and air-broadening coefficients, *J. Mol. Spectrosc.*, 212, 57-82, 2002.

8 Boone, C. D., Walker, K. A., Bernath, P. F., Version 3 retrievals for the Atmospheric Chemistry  
9 Experiment Fourier Transform Spectrometer (ACE-FTS). The Atmospheric Chemistry  
10 Experiment ACE at 10: A Solar Occultation Anthology, P. F. Bernath (Editor), A. Deepak  
11 Publishing, Hampton, Virginia, 2013.

12 Brewer, A. W.: Evidence for a world circulation provided by the measurements of helium and  
13 water vapour distribution in the stratosphere, *Q. J. Royal Met. Soc.*, 75, 351-363, 1949.

14 Cai, M. and Ren, R.-C., Meridional and downward propagation of atmospheric circulation  
15 anomalies. Part I: Northern hemisphere cold season variability, *J. Atmos. Sci.*, 1880-1901, 2007.

16 Carleer, M., Boone, C. D., Walker, K. A., Bernath, P. F., Strong, K., Sica, R. J., Randall, C. E.,  
17 Vömel, H., Kar, J., Höpfner, M., Milz, M., von Clarmann, T., Kivi, R., Valverde-Canossa, J.,  
18 Sioris, C. E., Izawa, M. R. M., Dupuy, E., McElroy, C. T., Drummond, J. R., Nowlan, C. R.,  
19 Zou, J., Nichitiu, F., Lossow, S., Urban, J., Murtagh, D., and Dufour, D. G.: Validation of water  
20 vapour profiles from the Atmospheric Chemistry Experiment (ACE), *Atmos. Chem. Phys.*  
21 *Discuss.*, 8, 4499-4559, 2008.

22 Chen, M., Rood, R. R., Read, W. G.: Seasonal variations of upper tropospheric water vapor and  
23 high clouds observed from satellites, *J. Geophys. Res.*, 6193-6197, 1999.

24 Del Genio, A. D., Kovari Jr., W., Yao, M.-S.: Climatic implications of the seasonal variation of  
25 upper troposphere water vapor, *Geophys. Res. Lett.*, 21, 2701-2704, 1994.

26 Dessler, A. E., Hints, E. J., Weinstock, E. M., and Anderson, J. G., Chan, K. R.: Mechanisms  
27 controlling water vapor in the lower stratosphere: "A tale of two stratospheres", *J. Geophys.*  
28 *Res.*, 100, 23167-23172, 1995.

1 Dessler, A. E. and Sherwood, S. C.: A matter of humidity, *Science*, 323, 1020-1021, doi:  
2 10.1126/science.1171264, 2009.

3 Dessler, A. E., Schoeberl, M. R., Wang, T., Davis, S. M., and Rosenlof, K. H.: Stratospheric  
4 water vapor feedback, *Proc. Natl. Acad. Sci.*, 110, 8087–18091, 2013.

5 Devasthale, A., Tjernström, M., Caian, M., Thomas, M. A., Kahn, B. H., and Fetzer, E. J.:  
6 Influence of the Arctic Oscillation on the vertical distribution of clouds as observed by the A-  
7 Train constellation of satellites, *Atmos. Chem. Phys.*, 12, 10535–10544, 2012.

8 Gettelman, A., Weinstock, E. M., Fetzer, E. J., Irion, F. W., Eldering, A., Richard, E. C.,  
9 Rosenlof, K. H., Thompson, T. L., Pittman, J. V., Webster, C. R., and Herman, R. L.: Validation  
10 of Aqua satellite data in the upper troposphere and lower stratosphere with in situ aircraft  
11 instruments, *Geophys. Res. Lett.*, 31, L22107, doi:10.1029/2004GL020730, 2004.

12 Groves, D. G., Francis, J. A.: Variability of the Arctic atmospheric moisture budget from TOVS  
13 satellite data, *J. Geophys. Res.* 107(D24), 4785, doi:10.1029/2002JD002285, 2002.

14 Hartmann, D. L., Klein Tank, A. M. G., Rusticucci, M., Alexander, L.V., Brönnimann, S.,  
15 Charabi, Y., Dentener, F. J., Dlugokencky, E. J., Easterling, D. R., Kaplan, A., Soden, B. J.,  
16 Thorne, P. W., Wild M., and Zhai, P.M.: Observations: Atmosphere and Surface. In: *Climate*  
17 *Change 2013: The Physical Science Basis. Contribution of Working Group I to the Fifth*  
18 *Assessment Report of the Intergovernmental Panel on Climate Change* [Stocker, T.F., D. Qin,  
19 G.-K. Plattner, M. Tignor, S.K. Allen, J. Boschung, A. Nauels, Y. Xia, V. Bex and P.M. Midgley  
20 (eds.)]. Cambridge University Press, Cambridge, United Kingdom and New York, NY, USA,  
21 2013.

22 Hegglin, M. I., Tegtmeier, S., Anderson, J., Froidevaux, L., Fuller, R., Funke, B., Jones, A.,  
23 Lingenfelser, G., Lumpe, J., Pendlebury, D., Remsberg, E., Rozanov, A., Toohey, M., Urban, J.,  
24 von Clarmann, T., Walker, K. A., Wang, R., and K. Weigel: SPARC Data Initiative: Comparison  
25 of water vapor climatologies from international satellite limb sounders, *J. Geophys. Res. Atmos.*,  
26 118, 11824-11846, doi:10.1002/jgrd.50752, 2013.

27 Herbin, H., Hurtmans, D., Clerbaux, C., Clarisse, L., and Coheur, P.-F.: H<sub>2</sub><sup>16</sup>O and HDO  
28 measurements with IASI/MetOp, *Atmos. Chem. Phys.*, 9, 9433–9447, 2009.

1 Hess, P. G., and Lamarque, J.-F.: Ozone source attribution and its modulation by the Arctic  
2 oscillation during spring months, *J. Geophys. Res.*, 112, D11303, doi:10.1029/2006JD007557,  
3 2007.

4 Highwood, E. J., Hoskins, B. J., and Berrisford, P.: Properties of the Arctic tropopause, *Quart. J.*  
5 *Roy. Meteorol. Soc.*, 126, 1515-1532, 2000.

6 Jakobson, E. and Vihma, T.: Atmospheric moisture budget in the Arctic based on the ERA-40  
7 reanalysis, *Int. J. Climatol.* 30, 2175–2194, 2010.

8 Lacis, A. A., Schmidt, G. A., Rind, D., Ruedy, R. A.: Atmospheric CO<sub>2</sub>: Principal control knob  
9 governing Earth's temperature, *Science*, 330, 356-359, 2010.

10 Lambert, A., Read, W. G., Livesey, N. J., Santee, M. L., Manney, G. L., Froidevaux, L., Wu, D.  
11 L., Schwartz, M. J., Pumphrey, H. C., Jimenez, C., Nedoluha, G. E., Cofield, R. E., Cuddy, D.  
12 T., Daffer, W. H., Drouin, B. J., Fuller, R. A., Jarnot, R. F., Knosp, B. W., Pickett, H. M., Perun,  
13 V. S., Snyder, W. V., Stek, P. C., Thurstans, R. P., Wagner, P. A., Waters, J. W., Jucks, K. W.,  
14 Toon, G. C., Stachnik, R. A., Bernath, P. F., Boone, C. D., Walker, K. A., Urban, J., Murtagh,  
15 D., Elkins, J. W., and Atlas, E.: Validation of the Aura Microwave Limb Sounder middle  
16 atmosphere water vapor and nitrous oxide measurements, *J. Geophys. Res.*, 112, D24S36, doi:  
17 10.1029/2007JD008724, 2007.

18 Laroche, S., Gauthier, P., St-James, J., Morneau, J.: Implementation of a 3D variational data  
19 assimilation system at the Canadian Meteorological Centre. Part II: The regional analysis,  
20 *Atmos. Ocean*, 37, 281–307, 1999.

21 Larson, J., Zhou, Y., Higgins, R. W.: Characteristics of landfalling tropical cyclones in the  
22 United States and Mexico: Climatology and interannual variability, *J. Clim.*, 18, 1247-1262,  
23 2005.

24 Li, Y., Thompson, D. W. J., Huang, Y., Zhang, M.: Observed linkages between the northern  
25 annular mode/North Atlantic Oscillation, cloud incidence, and cloud radiative forcing, *Geophys.*  
26 *Res. Lett.*, 41, 1681–1688, doi:10.1002/2013GL059113, 2014.

27 Lumpe, J., Bevilacqua, R., Randall, C., Nedoluha, G., Hoppel, K., Russell, J., Harvey, V. L.,  
28 Schiller, C., Sen, B., Taha, G., Toon, G., and Vömel, H.: Validation of Polar Ozone and Aerosol

1 Measurement (POAM) III version 4 stratospheric water vapor, *J. Geophys. Res.*, 111, D11301,  
2 doi:10.1029/2005JD006763, 2006.

3 McElroy, C. T., Nowlan, C. R., Drummond, J. R., Bernath, P. F., Barton, D. V., Dufour, D. G.,  
4 Midwinter, C., Hall, R. B., Ogyu, A., Ullberg, A., Wardle, D. I., Kar, J., Zou, J., Nichitiu, F.,  
5 Boone, C. D., Walker, K. A., and Rowlands, N.: The ACE-MAESTRO instrument on SCISAT:  
6 description, performance, and preliminary results, *Appl. Opt.*, 46, 4341–4356, 2007.

7 Mo, K. C.: Relationships between low-frequency variability in the southern hemisphere and sea  
8 surface temperature anomalies. *J. Clim.*, 13, 3599-3610, 2000.

9 Moss, A., Sica, R. J., McCullough, E., Strawbridge, K., Walker, K., and Drummond, J.:  
10 Calibration and validation of water vapour lidar measurements from Eureka, Nunavut, using  
11 radiosondes and the Atmospheric Chemistry Experiment Fourier Transform Spectrometer,  
12 *Atmos. Meas. Tech.*, 6, 741–749, 2013.

13 Murray, F. W.: On the computation of saturation vapor pressure, *J. Appl. Meteorol.*, 6, 203-204,  
14 1967.

15 Nedoluha, G. E., Bevilacqua, R. M., Hoppel, K. W., Lumpe, J. D., and Smit, H.: Polar Ozone  
16 and Aerosol Measurement III measurements of water vapor in the upper troposphere and  
17 lowermost stratosphere, *J. Geophys. Res.*, 107, ACH 7-1 – ACH 7-10, 10.1029/2001JD000793,  
18 2002.

19 Oman, L., Waugh, D. W., Pawson, S., Stolarski, R. S., and Nielsen, J. E.: Understanding the  
20 changes of stratospheric water vapor in coupled chemistry–climate model simulations, *J. Atmos.*  
21 *Sci.*, 65, 3278-3291, 2008.

22 Randel W. J., Moyer E., Park M., Jensen E., Bernath P., Walker K., and Boone C.: Global  
23 variations of HDO and HDO/H<sub>2</sub>O ratios in the upper troposphere and lower stratosphere derived  
24 from ACE-FTS satellite measurements, *J. Geophys. Res.*, 117, D06303,  
25 doi:10.1029/2011JD016632, 2012.

26 Shi, L., and Bates, J. J.: Three decades of intersatellite-calibrated High-Resolution Infrared  
27 Radiation Sounder upper tropospheric water vapor, *J. Geophys. Res.*, 116, D04108,  
28 doi:10.1029/2010JD014847, 2011.

1 Sioris, C. E., Zou, J., McElroy, C. T., McLinden, C. A., Vömel, H.: High vertical resolution water  
2 vapour profiles in the upper troposphere and lower stratosphere retrieved from MAESTRO solar  
3 occultation spectra, *Adv. Space Res.*, 46, 642–650, 2010.

4 Sioris, C. E., Zou, J., McElroy, C. T., Boone, C. D., Sheese, P. E., and Bernath, P. F.: Water  
5 vapour variability in the high-latitude upper troposphere – Part 2: Impact of volcanic eruptions,  
6 *Atmos. Chem. Phys.*, 16, x-y, 2016.

7 Soden, B.J., Jackson, D. L., Ramaswamy, V., Schwarzkopf, M. D., Huang, X.: The radiative  
8 signature of upper tropospheric moistening, *Science*, 310, 841-844, 2005.

9 Soden, B. J. and Held, I. M.: An assessment of climate feedbacks in coupled ocean-atmosphere  
10 models, *J. Clim.*, 19, 3354-3360, doi:10.1175/JCLI3799.1, 2006.

11 Steinbrecht, W., Köhler, U., Claude, H., Weber, M., Burrows, J. P., and van der A, R. J.: Very  
12 high ozone columns at northern mid-latitudes in 2010, *Geophys. Res. Lett.* 38: L06803,  
13 doi:10.1029/2010GL046634, 2011.

14 Su, H., Read, W. G., Jiang, J. H., Waters, J. W., Wu, D. L., and Fetzer, E. J.: Enhanced positive  
15 water vapor feedback associated with tropical deep convection: New evidence from Aura MLS,  
16 *Geophys. Res. Lett.*, 33, L05709, doi:10.1029/2005GL025505, 2006.

17 Suen, J. Y., Fang, M. T., and Lubin, P. M.: Global distribution of water vapor and cloud cover  
18 sites for high-performance THz applications, *IEEE Trans. Terahertz Sci. Technol.*, 4, 86-100,  
19 2014.

20 Thompson, D. W. J., Wallace, J. M.: Annular modes in the extratropical circulation. Part I:  
21 Month-to-month variability, *J. Clim.*, 13, 1000-1016, 2000.

22 Toohey, M., Hegglin, M. I., Tegtmeier, S., Anderson, J., Añel, J. A., Bourassa, A., Brohede, S.,  
23 Degenstein, D., Froidevaux, L., Fuller, R., Funke, B., Gille, J., Jones, A., Kasai, Y., Krüger, K.,  
24 Kyrölä, E., Neu, J. L., Rozanov, A., Smith, L., Urban, J., von Clarmann, T., Walker, K. A., and  
25 R. H. J. Wang: Characterizing sampling biases in the trace gas climatologies of the SPARC Data  
26 Initiative, *J. Geophys. Res. Atmos.*, 118, 11847–11862, doi:10.1002/jgrd.50874, 2013.

27 Treffeisen, R., Krejci, R., Ström, J., Engvall, A. C., Herber, A., and Thomason, L., Humidity  
28 observations in the Arctic troposphere over Ny-Ålesund, Svalbard based on 15 years of  
29 radiosonde data, *Atmos. Chem. Phys.*, 7, 2721–2732, 2007.



1 Waymark, C., Walker, K. A., Boone, C. D., and Bernath, P. F.: ACE-FTS version 3.0 data set:  
2 validation and data processing update, *Annals of Geophys.*, 56, doi:10.4401/ag-6339, 2013.

3 Wiegele, A., Schneider, M., Hase, F., Barthlott, S., García, O. E., Sepúlveda, E., González, Y.,  
4 Blumenstock, T., Raffalski, U., Gisi, M., and Kohlhepp, R.: The MUSICA MetOp/IASI H<sub>2</sub>O and  
5  $\delta$ D products: characterisation and long-term comparison to NDACC/FTIR data, *Atmos. Meas.*  
6 *Tech.*, 7, 2719–2732, 2014.

7 Worden, J., Kulawik, S. S., Shephard, M. W., Clough, S. A., Worden, H., Bowman, K., and  
8 Goldman, A.: Predicted errors of tropospheric emission spectrometer nadir retrievals from  
9 spectral window selection, *J. Geophys. Res.*, 109, D09308, doi:10.1029/2004JD004522, 2004.

10

11

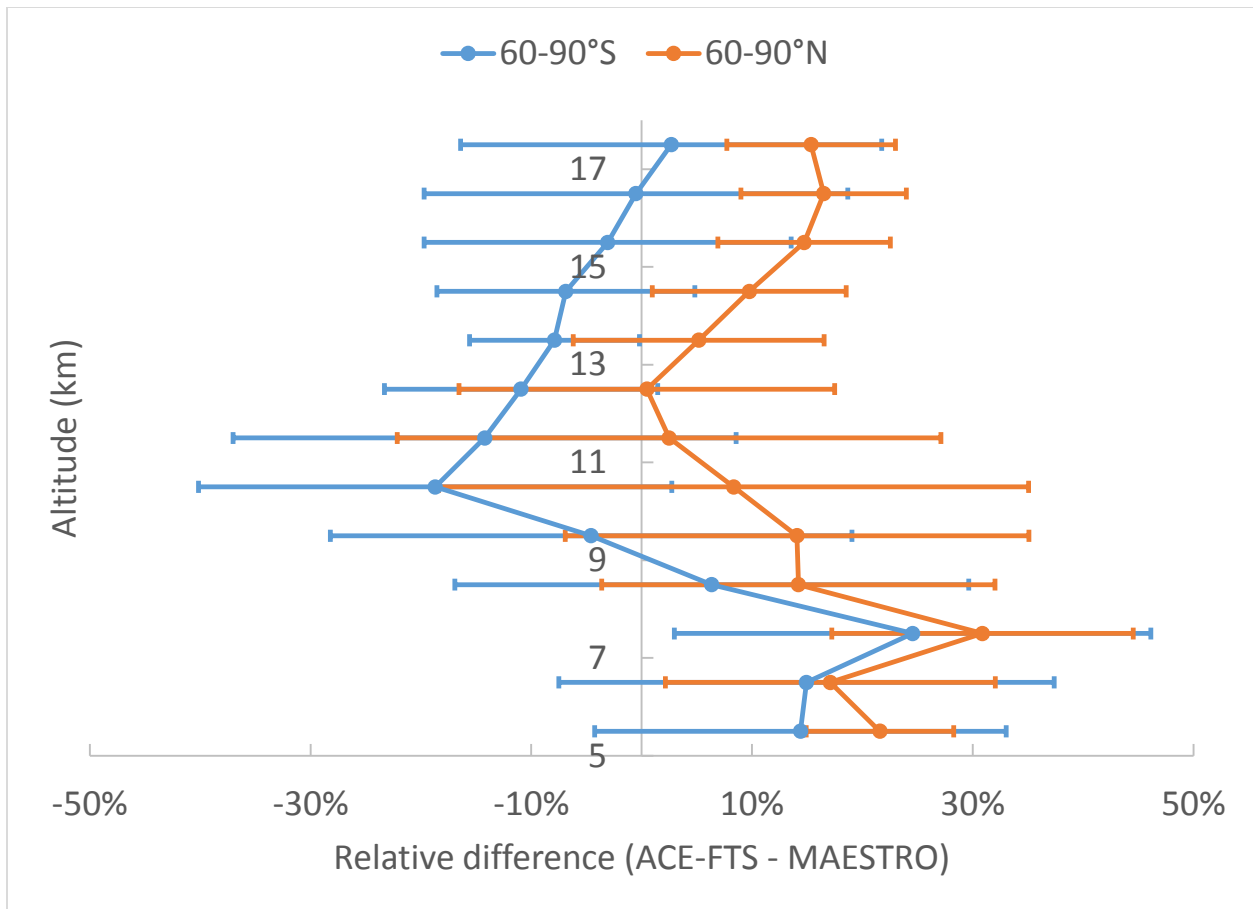
12

13

14

15

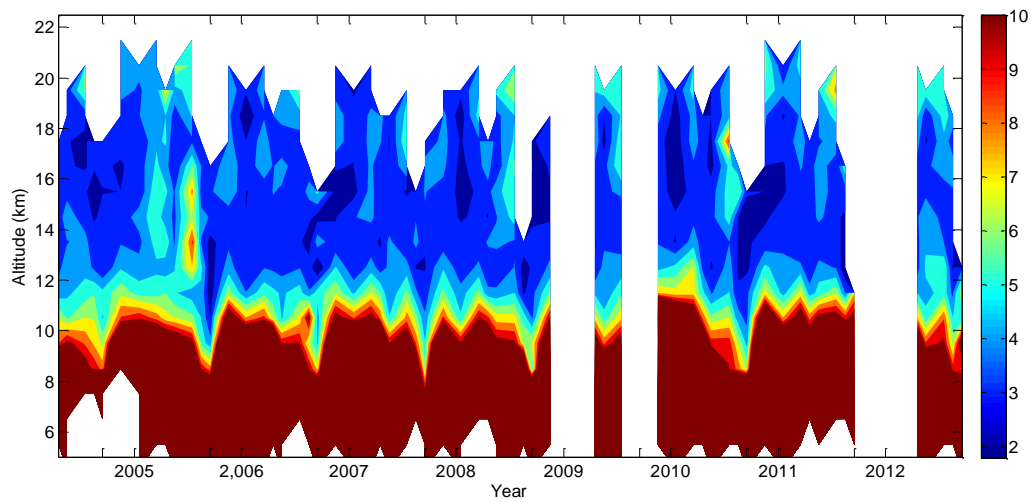
16



1

2 Figure 1. (orange) Relative differences between ACE-FTS and MAESTRO climatological  
 3 medians averaged over the eight months sampling the northern high-latitude region and their  
 4 standard deviation; (blue) relative differences between ACE-FTS and MAESTRO climatological  
 5 means averaged over the eight months sampling the southern high-latitude region and their  
 6 standard deviation. The horizontal bars show the standard deviation of the differences between  
 7 the two climatologies over the eight available months. To account for vertical resolution  
 8 differences, the MAESTRO climatology was vertically smoothed with a 3 km boxcar.

9



1

2 Figure 2. Time series of the MAESTRO monthly mean water vapour volume mixing ratio  
 3 (VMR) versus altitude (5.5-22.5 km) at southern high latitudes (60-90°S) with a linear colour  
 4 scale (ppm), emphasizing the stratospheric variability. Unlabelled ticks along the bottom  
 5 correspond to September. The time series is composed using the eight months in which ACE  
 6 samples the southern high latitudes (see Sect. 2.4).

7

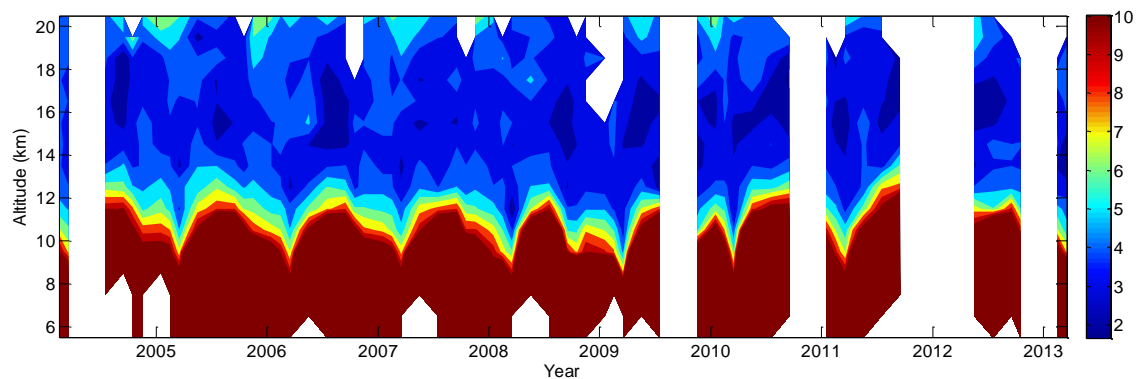
8

9

10

11

12



1

2 Figure 3. Time series of the MAESTRO monthly median water vapour volume mixing ratio  
3 (VMR) versus altitude (km) at northern high latitudes (60-90°N). The time series is composed  
4 using the eight months in which ACE samples the northern high latitudes (see Sect. 2.4).

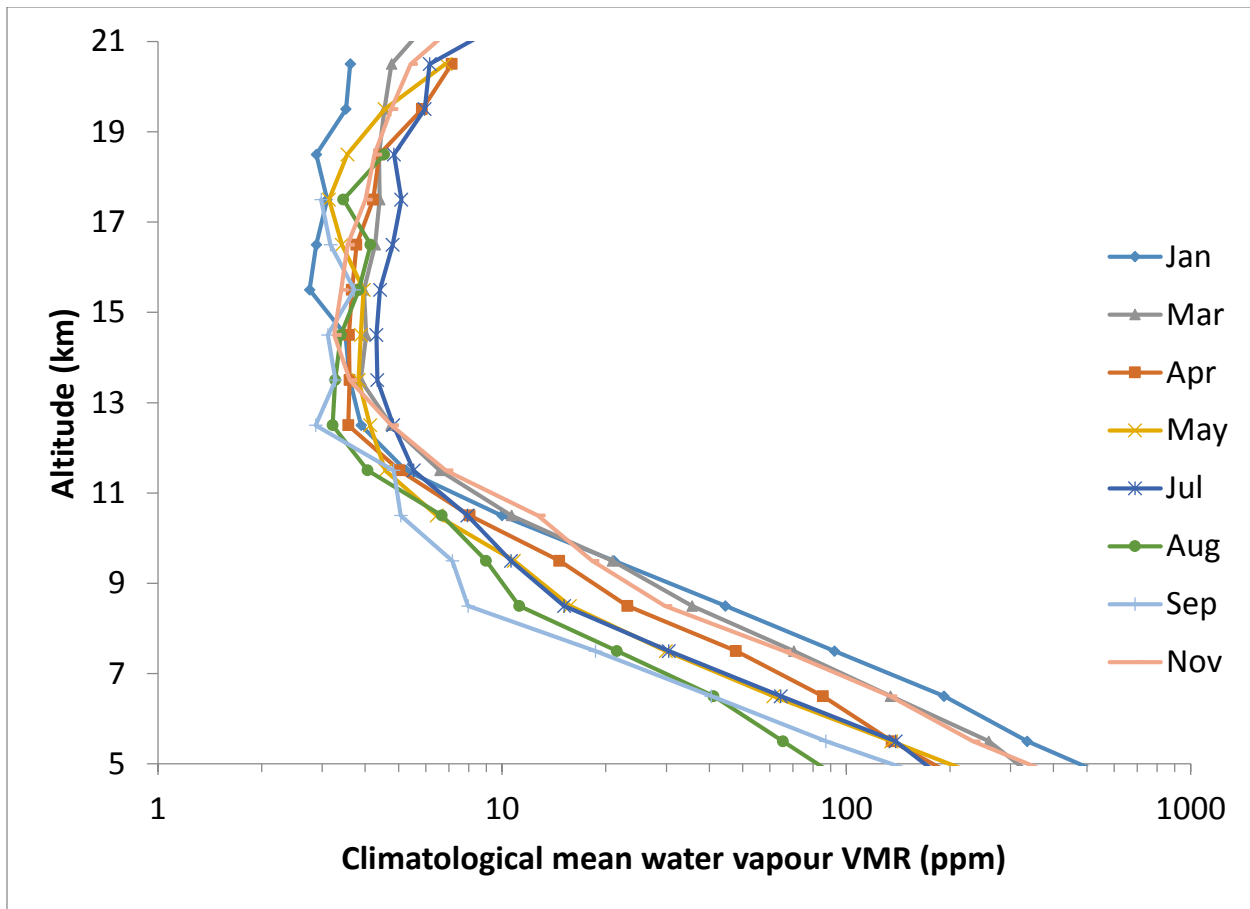
5

6

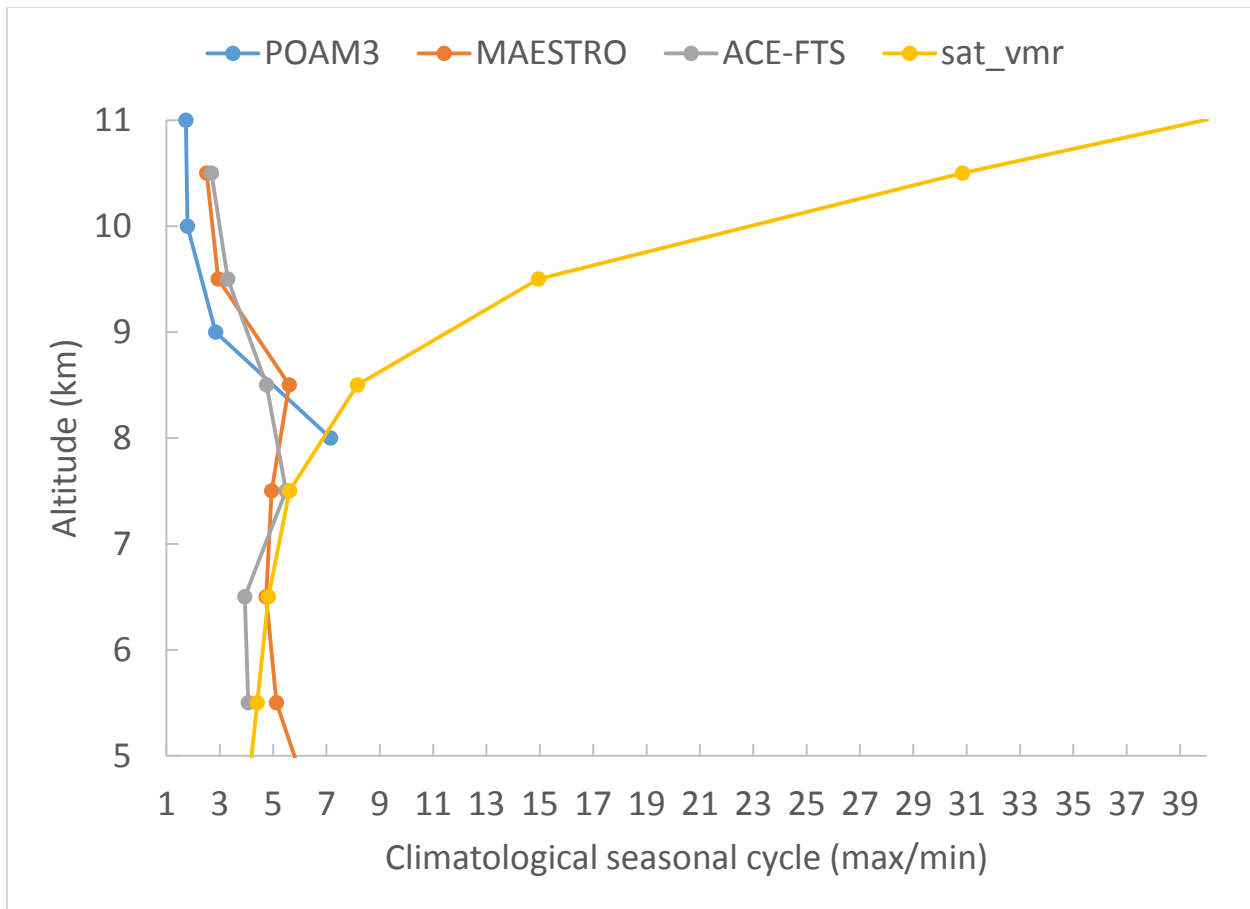
7

8

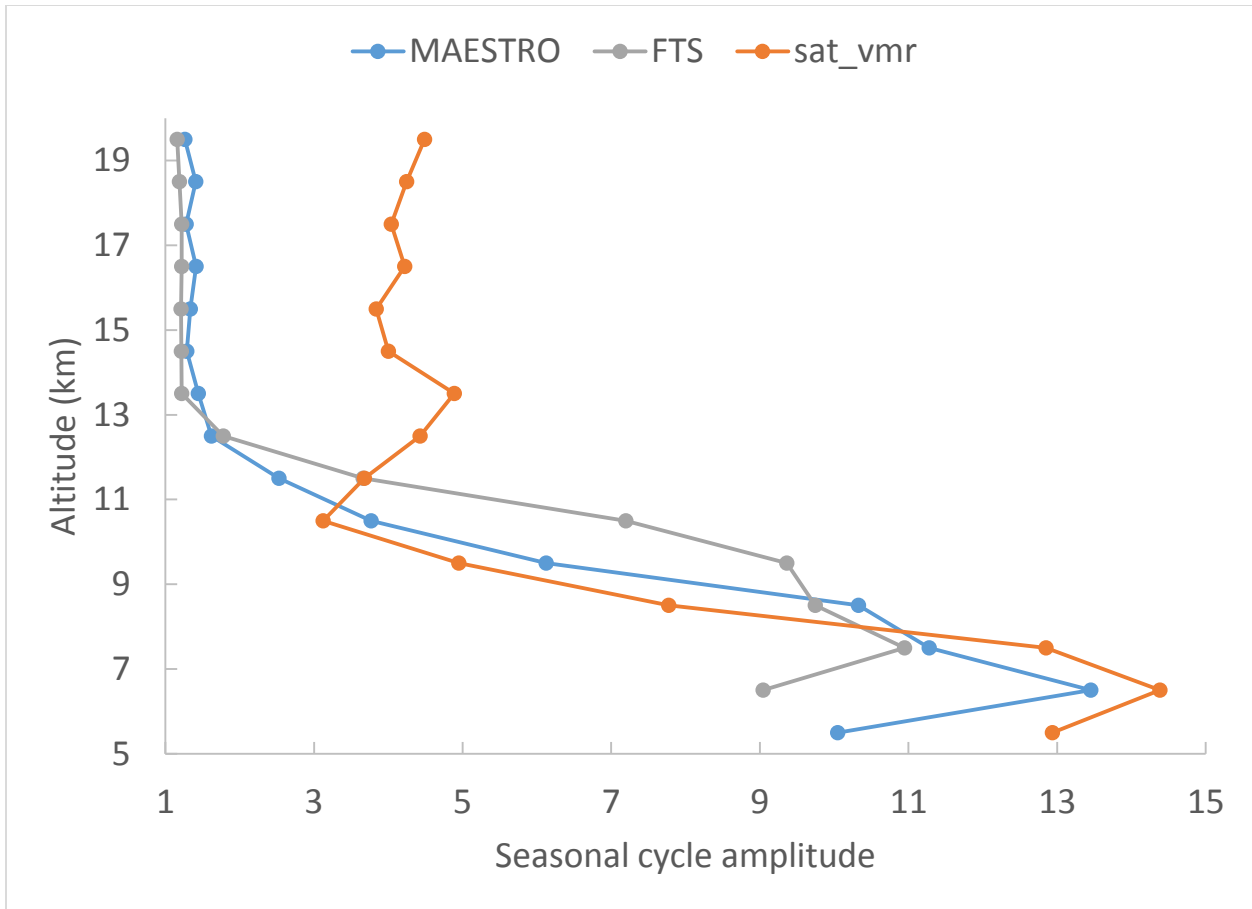
9



1  
 2 Figure 4. MAESTRO mean climatology (2004-2012) of the vertical distribution of water vapour  
 3 volume mixing ratio in the Antarctic (60-90°S) UT/LS for months with sufficient sampling of  
 4 the region. A logarithmic scale is used for the x-axis.

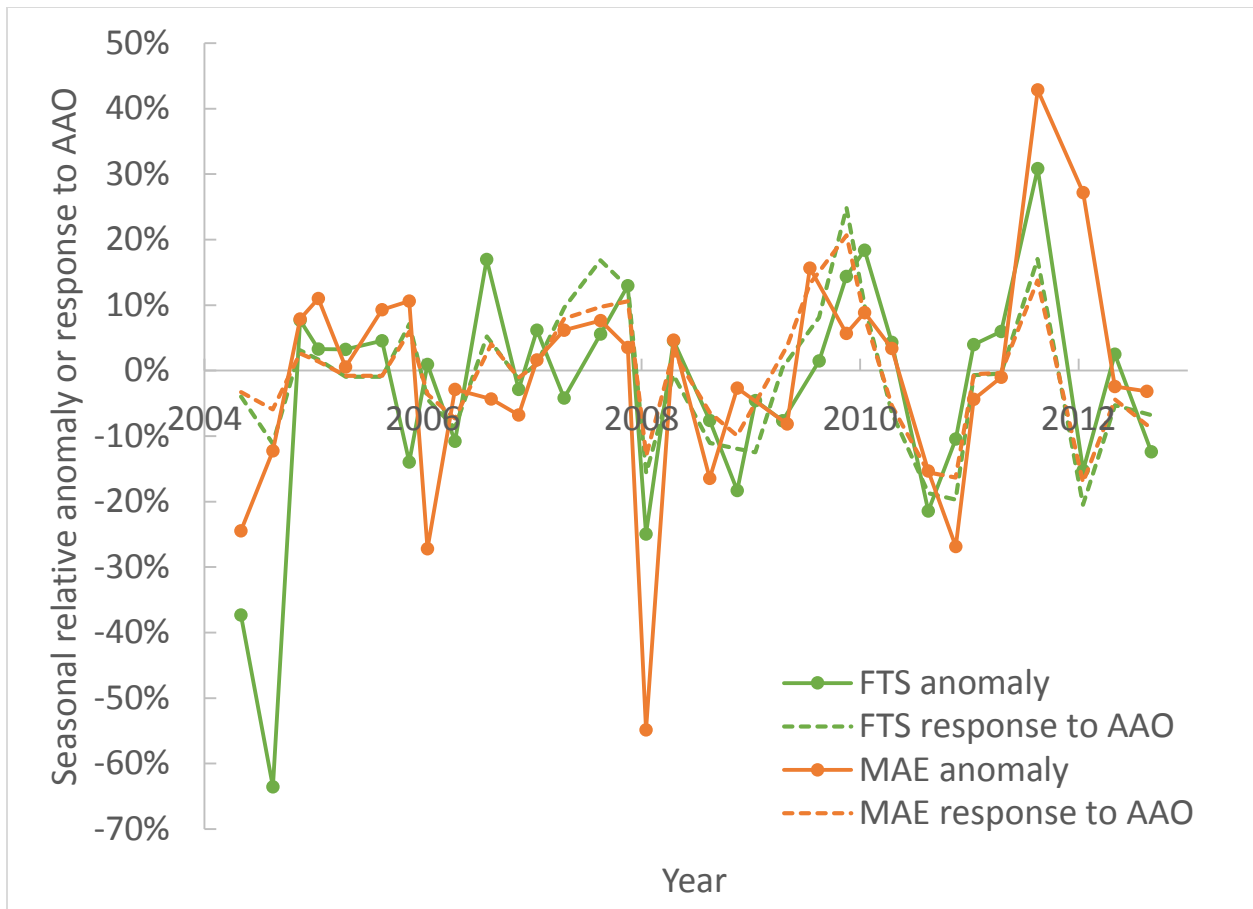


1  
 2 Figure 5. Vertical profile of the seasonal cycle amplitude of Antarctic water vapour observed by  
 3 three instruments. The amplitude is calculated by taking the ratio of climatological monthly  
 4 means at maximum (January or December) and minimum (August or September). Note that  
 5 POAM III has a different orbit that tends to sample consistently at higher latitudes (Nedoluha et  
 6 al., 2002) and thus tends to have stronger seasonality at 8 km (driven by the larger temperature  
 7 range). The saturation vapour pressure climatology is obtained using GEM analysis  
 8 temperatures sampled at ACE measurement locations.



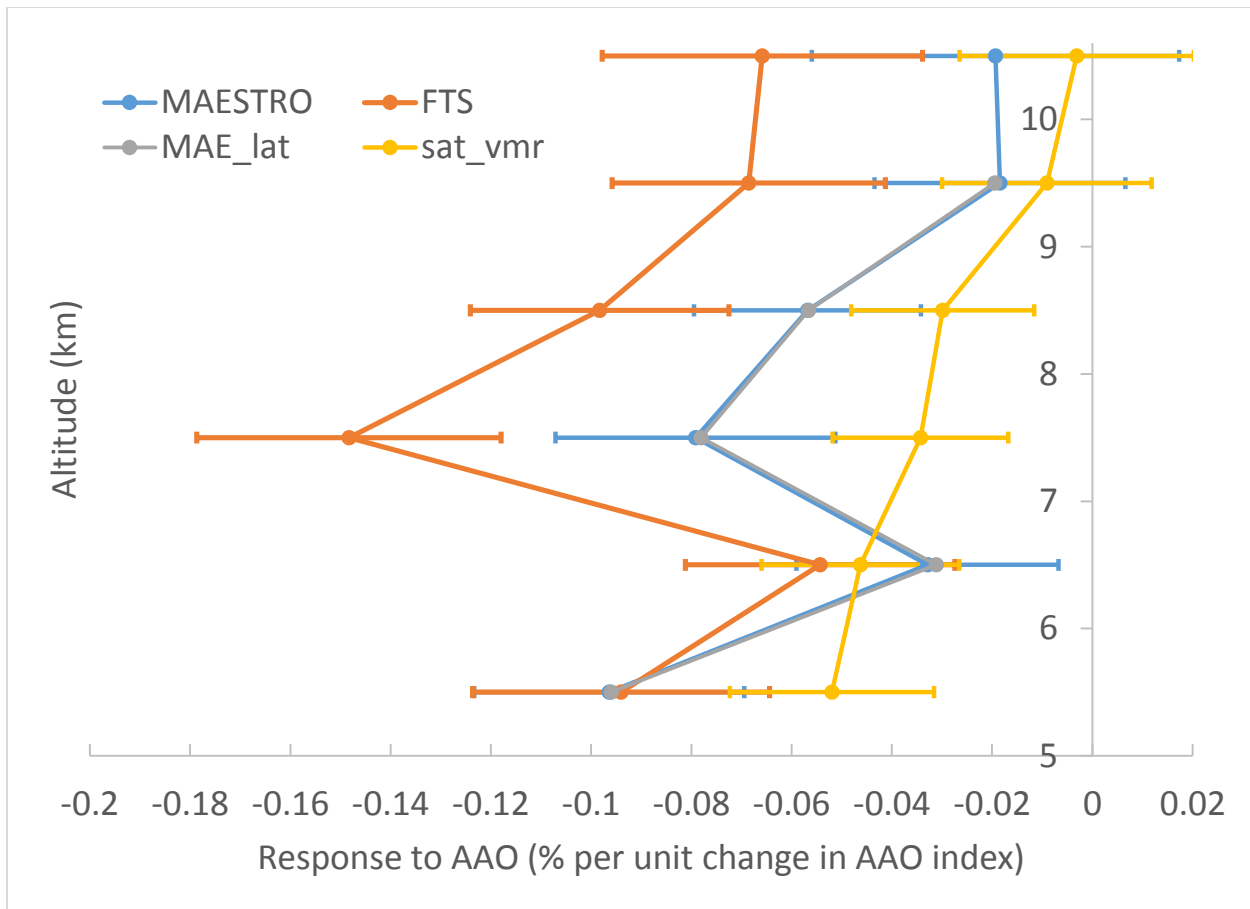
1

2 Figure 6. Analogous to Fig. 5 but for northern high latitudes. Profiles are presented at their  
 3 respective native vertical resolutions.



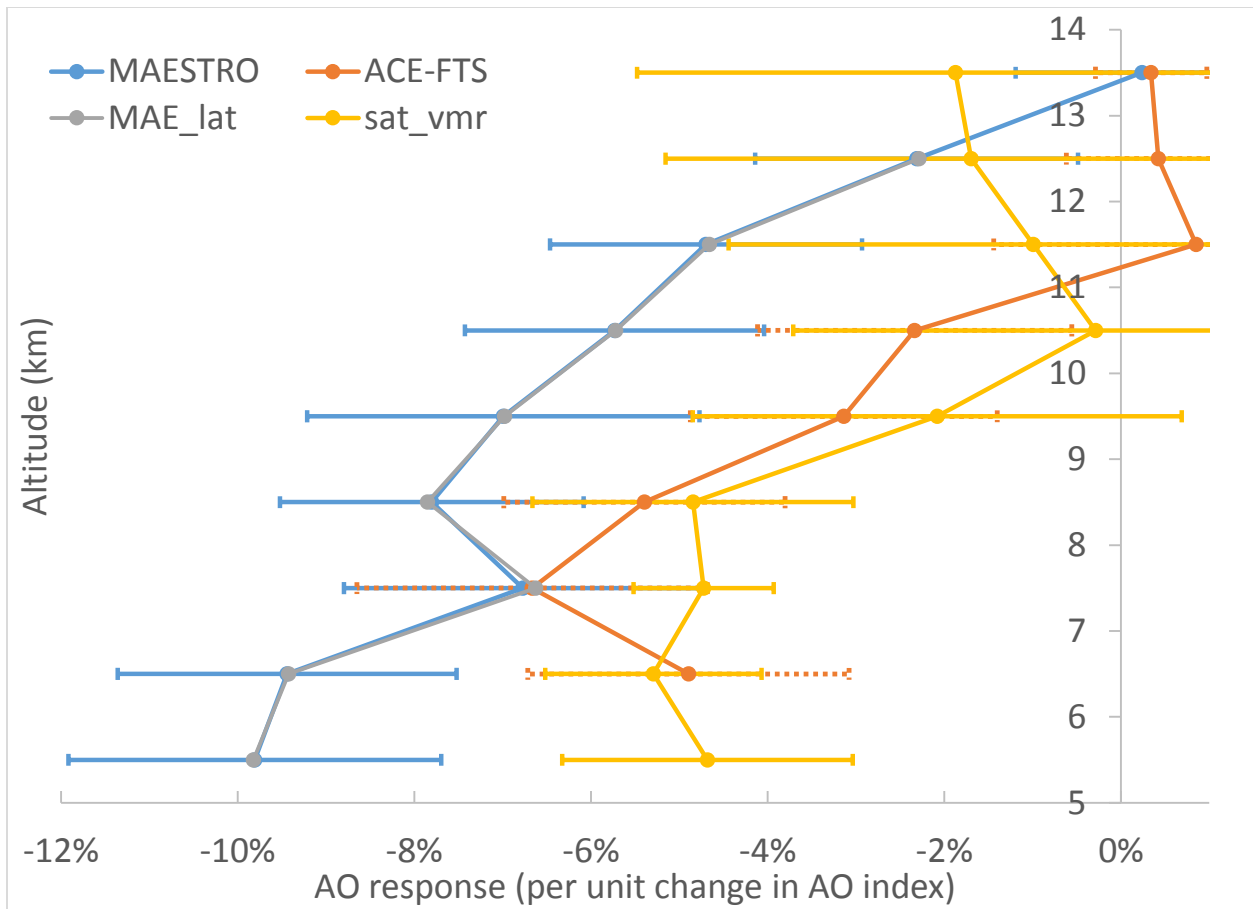
1  
 2 Figure 7. Seasonal median water vapour anomaly time series from MAESTRO (8.5 km) and  
 3 ACE-FTS (7.5 km) in the Antarctic troposphere and the response of each to AAO determined by  
 4 linear regression. Seasons with missing data are removed to avoid discontinuities. The markers  
 5 on the response curves indicate the sampled seasons.





1  
 2 Figure 8. Vertical profile of response to AAO, using southern high latitude water vapour relative  
 3 anomalies based on monthly medians (2004-2012). Horizontal bars are  $\pm 1\sigma$ , obtained by linear  
 4 regression (including a trend term and/or a Puyehue proxy term depending on whether each is  
 5 significant at the  $1\sigma$  level). The “MAE\_lat” profile shows the MAESTRO water vapour response  
 6 to AAO upon including a basis function to account for the non-uniform latitudinal sampling. The  
 7 ‘sat\_vmr’ profile is obtained from a simple linear regression of saturation vapour VMR relative  
 8 anomalies onto AAO.

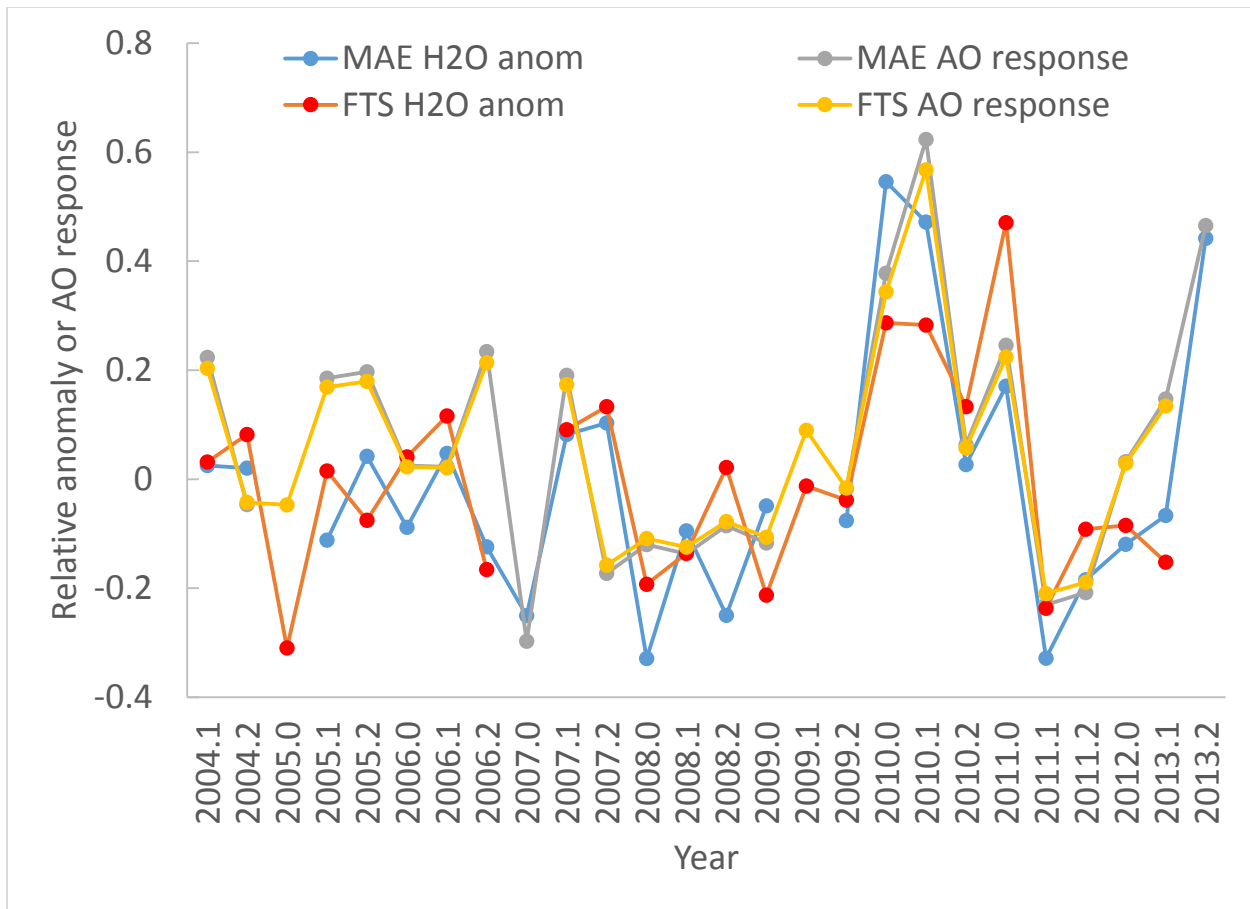
9



1

2 Figure 9. Analogous to Fig. 8, but for northern high latitudes water vapour in response to the  
 3 Arctic oscillation. Error bars display  $\pm 1$  standard error of the fitting coefficient for the AO index  
 4 obtained by linear regression. At 5.5 km, the response of ACE-FTS is not shown since it has a  
 5 standard error of  $>100\%$  and the sample size decreases significantly.

6



1  
 2 Figure 10. Time series of water vapour relative anomalies observed by ACE-MAESTRO  
 3 (“MAE”) and ACE-FTS at 6.5±0.5 km in winter months (January-March). Slight differences in  
 4 sampling exist between the two instruments due to the requirement for >20 observations per  
 5 month per altitude bin.